A: Kinetics, Dynamics, Photochemistry, and Excited States

Photoinduced Reactivity in a dispiro-1,2,4-trioxolane: Adamantane Ring Expansion and First Direct Observation of the Long-lived Triplet Diradical Intermediates

Elisa M. Brás, Lília Isabel Lameirinhas Cabral, Patrícia Sofia Menalha Amado, Manabu Abe, Rui Fausto, and Maria Lurdes Santos Cristiano

Just Accepted

1 **Photoinduced reactivity in a dispiro-1,2,4-trioxolane: adamantane ring**

2 **expansion and first direct observation of the long-lived triplet diradical**

3 **intermediates**

4

5 Elisa M. Brás,[a,c] Lília I. L. Cabral,[a,b] Patrícia S. M. Amado,[a,b] Manabu Abe,[d] Rui Fausto[c,*]

6 and Maria L. S. Cristiano[a,b,*]

7

8   [a] *Centro de Ciências do Mar (CCMAR), Universidade do Algarve, Campus Gambelas, Faro, Portugal.*

9   [b] *Departamento de Química e Farmácia, Faculdade de Ciências e Tecnologia, Universidade do Algarve,*

10 *Campus de Gambelas, Faro, Portugal.* [c] *CQC, Department of Chemistry, University of Coimbra, Portugal.*

11   [d] *Department of Chemistry, Graduate School of Science, Hiroshima University, Hiroshima, Japan.*

12

13 **ABSTRACT**

14

15 The dispiro-1,2,4-trioxolane **1**, an ozonide with efficient and broad antiparasitic activity, was

16 synthesized and investigated using matrix isolation FTIR and EPR spectroscopies together

17 with both B3LYP/6-311++G(3df,3dp) and M06-2X/6-311++G(3df,3dp) theoretical

18 methods. Irradiations ($\lambda \geq 290$ nm) of the matrix isolated **1** (Ar or N_2) afforded exclusively

19 4-oxahomoadamantan-5-one **4** and 1,4-cyclohexanedione **5**. These results suggested that the

20 reaction proceeded *via* a dioxygen-centered diradical intermediate, formed upon homolytic

21 cleavage of the labile peroxide bond, which regioselectively isomerized to form the more

22 stable (secondary carbon-centered)/oxygen-centered diradical. *In situ* EPR measurements

23 during the photolysis of **1** deposited in a MeTHF-matrix led to the detection of signals

24 corresponding to two triplet species, one of which was short-lived while the other proved to

25 be persistent at 10 K. These observations strongly support the proposed mechanism for the

26 photogeneration of **4** and **5**, which involves intramolecular rearrangement of the intermediate

27 diradical species **2** to afford the triplet diradical **3**.

28

29 * Corresponding authors e-mails:

30 R.F.: rfausto@ci.uc.pt

31 M.L.S.C.: mcristi@ualg.pt

32

INTRODUCTION

Organic dispiro-endoperoxides, in particular dispiro 1,2,4-trioxanes and 1,2,4-trioxolanes (ozonides), have been attracting much attention since the discovery of artemisinin more than 40 years ago[1-3], which provided a completely new antimalarial structural prototype of pharmacophore. The mechanism of bioactivation and action of the artemisinins and related endoperoxide based drugs has been discussed thoroughly[4-14] and bioactivation is known to require iron(II)-induced reductive cleavage of the peroxide bond to form oxygen-centered radicals, followed by rearrangement to generate carbon-centered radical species that act through modification of parasites biological targets. From a synthetic point of view, endoperoxides are useful for preparation of different types of compounds *via* ring expansion reactions[15], and also for the synthesis of α-keto acids[16] *cis*-diols[17], 1,2-diol monoesters[18,19], benzofurans and benzopyrans[20] *via* selective ring cleavage.

In all the above chemical processes, radical or diradical species have been hypothesized to be the key reactive intermediates, following the initial homolytic cleavage step. For asymmetrically substituted dispiro-1,2,4-trioxolanes, represented by compound **1**, and also for their dispiro-1,2,4-trioxane analogues, it has been postulated, based on the final reaction products obtained, that after the cleavage of the peroxide bond generating the dioxygen-centered diradical **2** a regioselective β-scission occurs concomitantly with the rearrangement, leading to the carbon-centered/oxygen-centered diradical species **3** (see Scheme 1)[21-23].
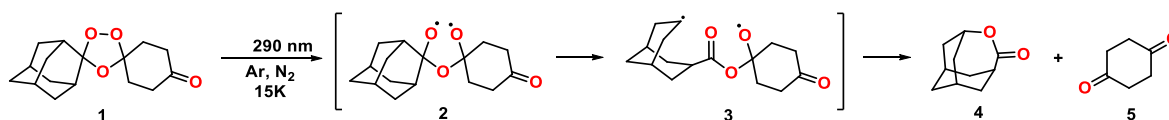
Scheme 1. Generic mechanistic scheme for a representative reaction of a dispiro-1,2,4-trioxolane starting with the homolytic cleavage of the O–O bond. The example chosen relates with the present study, where the reaction took place in a cryogenic matrix (either solid Ar or N_2, at 15 K), the substituents of the trioxolane core being the spiroadamantyl and spiro-*p*-cyclohexanonyl groups and using UV light ($\lambda \geq 290$ nm) as the reaction initiator.

When Fe(II) is involved in the reaction, as during the Fe(II)-induced cleavage of the antimalarial peroxides, the metal ion binds to the radical species[4-14]. In spite of the

2

62 accumulated evidence of the participation of radicals or diradicals in all these types of

63 reactions, and also of the successful detection of some of these species for reactions involving

64 cyclic peroxides[24, 25], the experimental detection and characterization of the diradical species

65 following the homolytic peroxide bond cleavage of dispiro-1,2,4-trioxolanes has not been

66 reported hitherto.

67   In the present article, we report the first direct observation of the two claimed diradical

68 intermediates for this type of reaction. The strategy used to achieve this goal started with the

69 identification of the final products of the UV-induced unimolecular photolysis of

70 adamantane-2-spiro-3'-8'-oxo-1',2',4'-trioxaspiro[4,5]decane (**1**) isolated in low

71 temperature matrices (argon and N_2), and their vibrational characterization. Subsequently,

72 the EPR spectroscopy was used to search for the involved diradicals generated under UV-

73 photolysis of the compound isolated in a low temperature MeTHF matrix. The choice for the

74 low temperature solid state media to perform this investigation was motivated by three main

75 reasons: (1) under these conditions, because the molecules of the precursor are cage-confined

76 and diffusion does not take place[26-30], no products can be expected to be formed resulting

77 from species produced from fragmentation of different molecules; this considerably

78 simplifies the accessible chemistry, thus allowing to focus on the main features of the

79 mechanism of the reaction; (2) due to the low work temperature (of a few K) the attainable

80 spectral resolution is much higher compared to what can be obtained, for example, in

81 solution[26-30]; together with absence of significant interactions with the host material this

82 feature allowed to obtain data of better quality for structural elucidation and, at the same

83 time, that could be directly compared with results of quantum chemical computational

84 predictions, which were done for the isolated molecules *in vacuo*; (3) finally, it could also be

85 expected that the lifetime of the intermediates were longer under the used experimental

86 conditions (low temperature; inhibited molecular diffusion; relative inertness of the

87 medium), so that their experimental detection would be facilitated.

88   As described in detail below, the obtained results demonstrate that the UV-induced

89 photolysis of the investigated dispiro-1,2,4-trioxolane proceeds regioselectively, leading to

90 its adamantane substituent ring expansion, *via* the two key diradical triplet species suggested

91 previously, which could be successfully detected here for the first time by EPR spectroscopy.

92 As it could be expected, the measured lifetimes of the two diradicals differ considerably, with

93   the carbon-centered/oxygen-centered diradical being considerably more stable than its

94   oxygen centered diradical precursor.

95   It is worth noting that trioxolane **1** has very relevant and broad antiparasitic properties. It

96   has shown low nanomolar activity against *Plasmodium falciparum*[31] and recent studies

97   demonstrated that its activity is retained against *P. falciparum* strains resistant to chloroquine

98   and to the artemisinin-derived drugs used in combination therapies (ACT)[32]. Compound 1

99   also exhibits low micromolar activity against intracellular amastigote forms of *Leishmania*

100   *infantum*[33] and against *Perkinsus olseni*[34]. In addition to its broad antiparasitic activity, the

101   studied compound can be prepared from the commercially available 2-adamantanone and

102   1,4-cyclohexanedione building blocks in only 2 steps.

103

104   **EXPERIMENTAL AND COMPUTATIONAL DETAILS**

105   ***General***

106   Commercial reagents were used as purchased. ^{1}H and ^{13}C-NMR spectra were recorded

107   on a 400 MHz NMR spectrometer Bruker Avance III 400. ^{1}H-NMR-chemical shifts are

108   referred to the residual signal of CDCl$_3$ (δH 7.26) and ^{13}C-NMR-chemical shifts to the CDCl$_3$

109   signal (δC 77.0), or using TMS as internal standard. Thin-layer chromatography was carried

110   out on silica gel 60 F254 plates (AL TLC 20x20). Column chromatography was performed

111   on Silica Gel 60 (0.04 – 0.063 mm). Melting points (°C) were obtained on a SMP3 Melting

112   Point Apparatus and are uncorrected.

113

114   ***Syntheses and general characterization of the compounds***

115   **Adamantane-2-spiro-3'-8'-oxo-1',2',4'-trioxaspiro[4,5]decane 1**: ozone, produced

116   with an ozone generator Sander Labor-Ozonizator 301.7 (0.5 L/min O$_2$, 140 V), was passed

117   through a solution of dichloromethane at –78 °C and flushed into a solution of *O*-methyl 2-

118   adamantanone oxime (1.00 g, 5.58 mmol) and 1,4-cyclohexanedione (0.65 g, 5.58 mmol) in

119   pentane (60 mL) and dichloromethane (40 mL) at 0 °C. After consumption of the starting

120   material, the solution was flushed with nitrogen for 5 min and concentrated under reduced

121   pressure at room temperature to give a crude material. Purification by flash chromatography

122   using a mixture of EtOAc/*n*-hexane, gave the pure compound as a colorless solid (0.66 g,

123   42% yield): m.p. 127-128 °C; ^{1}H-NMR (400 MHz, CDCl$_3$): δ 1.69-2.02 (m, 14H), 2.14 (t, *J*

124   = 6.9 Hz, 4H), 2.51 (t, J = 7.0 Hz, 4H) ppm; ^{13}C-NMR (100 MHz, CDCl$_3$): 25.9, 26.31, 31.09,

125   32.59, 34.25, 35.70, 36.18, 37.35, 106.46, 111.95, 208.90 ppm; MS (EI, m/z): 278.9 [M]$^+$.

126   The *O*-methyl 2-adamantanone oxime precursor of compound **1** was obtained as follows:

127   to a solution of 2-adamantanone (4.00 g, 26.63 mmol) in methanol (20 mL), under stirring,

128   was added pyridine (3.40 mL, 42.03 mmol) and methoxylamine hydrochloride (2.846 g,

129   34.08 mmol). The reaction mixture was stirred at room temperature for 72 h. The final

130   mixture was concentrated and then diluted with dichloromethane (20 mL) and water (30 mL).

131   The organic layer was separated, and the aqueous layer was washed with dichloromethane

132   (2x20 mL). The combined organic layers were washed with aqueous HCl (1 M; 20 mL x2),

133   then with brine (20 mL). The final organic extract was dried with MgSO$_4$, filtered, then

134   concentrated under reduced pressure to give *O*-methyl-2-adamantanone oxime (4.20 g, 88%

135   yield) as a colorless solid (m.p. 69-70 °C). ^{1}H-NMR (400 MHz, CDCl$_3$): δ 3.81 (s, 3H), 3.46

136   (s,1H), 2.54 (s, 1H), 2.00 – 1.78 (m, 12H) ppm. ^{13}C NMR (101 MHz, CDCl$_3$) δ: 166.74,

137   60.96, 39.03, 37.64, 36.52, 36.24, 29.53, 27.85 ppm. MS (MALDI-TOF, m/z): 180.02 [M]$^+$.

138   **4-Oxahomoadamantan-5-one 4**, was synthesized using the procedure described by

139   Renoud-Grappin *et al*.[35] To a suspension of 2-adamantanone (0.5 g, 3.33 mmol) and NaHCO$_3$

140   (0.31 g, 3.66 mmol) in anhydrous dichloromethane (10 mL) was added a solution of *m*-

141   chloroperoxybenzoic acid (*m*-CPBA) (0.86 g, 4.99 mmol) in anhydrous dichloromethane (5

142   mL). The reaction mixture was stirred at room temperature, in the dark, until consumption of

143   the starting compound. Then the organic mixture was washed with water (3x15 mL), brine

144   (2x15 mL) and dried over with MgSO$_4$. The organic layer was then evaporated to dryness

145   under reduced pressure. Purification of the residue by flash chromatography using a mixture

146   of EtOAc/*n*-hexane, gave the required product as a white solid (0.35 g, 63% yield): m.p: 288-

147   290 °C. ^{1}H NMR (400 MHz, CDCl$_3$): δ = 4.49 (tt, J = 4.4, 2.4 Hz, 1H), 3.10 – 3.05 (m, 1H),

148   2.16 – 1.58 (m, 12H). ^{13}C NMR (101 MHz, CDCl$_3$): δ = 178.99, 73.17, 41.24, 35.78, 33.82,

149   30.96, 25.85. HRMS (CI, m/z) calcd for C$_{10}$H$_{15}$O$_2$ (M+H)$^+$: 167.1067; found 167.1072.

150   **1,4-Cyclohexanedione 5** was purchased from Sigma Aldrich UK and used without

151   further purification.

152   All compounds prepared were kept in the freezer and shielded from the light during

153   storage, remaining stable under these conditions.

154

155 ***Matrix isolation infrared spectroscopy measurements***

156   To prepare the low temperature matrices a sample of the solid compound to be studied

157 was placed in an especially designed thermoelectrically heatable mini-oven attached to the

158 vacuum chamber of a helium cryostat (APD Cryogenics closed-cycle helium refrigerator

159 system with a DE-202A expander). Before the measurements, the samples were subjected to

160 additional purification by continued high-vacuum ($\sim10^{-7}$ mbar) pumping, during

161 approximately 1 hour, at room temperature. The samples were then sublimed and the vapors

162 of the compound to be studied were deposited, together with a large excess of argon or N_2,

163 onto a cesium iodide (CsI) substrate mounted at the cryostat cold tip (15 ± 0.1 K, as measured

164 by a silicon diode sensor connected to a Scientific Instruments digital temperature controller).

165 This temperature was kept during the overall experiments.

166   The IR spectra of the matrix-isolated compounds were recorded in the $400-4000$ cm^{-1}

167 range and with 0.5 cm^{-1} spectral resolution, using a Nicolet 6700 Fourier transform infrared

168 (FTIR) spectrometer, equipped with a deuterated triglycine sulfate (DTGS) detector and a

169 Ge/KBr beam splitter. The optical bench was continuously purged with a flux of dry and CO_2

170 filtered N_2, to avoid interference from atmospheric H_2O and CO_2.

171 ***Matrix isolation EPR spectroscopy measurements***

172   A 100 mM solution of compound 1 in MeTHF (100 μL) was degassed under high vacuum

173 (~3.0 x 10^{-2} Pa) in a quartz EPR tube, which was sealed after three freeze-pump-thaw cycles

174 under the vacuum conditions. The MeTHF solution of compound 1 was irradiated in the EPR

175 cavity at 10 K. The X-band EPR signals were obtained at a resonance frequency of 9.40 GHz

176 using a Bruker E500 spectrometer at 10-50 K.

177

178 ***In situ UV irradiation experiments***

179   In the steady state infrared spectroscopy experiments carried out in Ar and N_2 matrices,

180 *in situ* UV irradiation of the samples was undertaken using different approaches. In the case

181 of the experiments carried out in the Ar matrices, broadband UV radiation was used, as

182 provided by the KBr external window of the cryostat and water filtered ($\geq$ 290 nm) light

183 generated by a 500 W Hg(Xe) lamp (Newport, Oriel Instruments), with output power set to

184 200 W. For the experiments carried out in the N_2 matrices, tunable narrowband light was

185 used (~0.1 cm^{-1} bandwidth; $\lambda = 290$ nm; pulse energy ~8 mJ), provided by a Spectra Physics

186   Quanta-Ray MOPO-SL optical parametric oscillator (OPO) pumped with a pulsed Nd:YAG

187   laser (repetition rate = 10 Hz, duration = 10 ns).

188   For the EPR measurements, the photolysis was conducted at 266 nm (5 mJ), using a Nd-

189   YAG laser (Spectra Physics Indi-40).

190

191   ***Computational Details***

192   Quantum chemistry computations were performed at both the B3LYP/6-

193   311++G(3df,3dp) and M06-2X/6-311++G(3df,3dp) levels of theory[36-43], using Gaussian 09

194   (Revision D.01)[44]. Geometry optimizations were performed using the "tight" optimization

195   criteria.

196   The harmonic vibrational wavenumbers and IR intensities were calculated at the same

197   levels of theory and scaled in order to correct them for the neglect of anharmonicity, basis

198   sets restraints and the effect of incomplete treatment of the electron correlation. The scaling

199   factors were acquired by fitting the computed harmonic to the experimental IR wavenumbers

200   of compound 1 within the 1900-600 cm^{-1} region and those of compounds **4** and **5** within the

201   1900-500 cm^{-1} (see Figure S1 in the Supporting Information). The slopes obtained by least-

202   squares linear fit, intercepting zero ($y = bx$), were then used to scale the computed harmonic

203   wavenumbers of the photoproducts and reactant in the 1900-400 cm^{-1} range. The simulation

204   of the IR spectra was achieved using the calculated (scaled) wavenumbers and IR intensities

205   (in km mol^{-1}), which were convoluted with Lorentzian functions with a full-width at half-

206   maximum (fwhm) of 2 cm^{-1}.

207

208   **RESULTS AND DISCUSSION**

209   ***Photoinduced reactivity of 1 in low temperature solid Ar and N$_2$ matrices***

210   B3LYP and M06-2X density functional theory calculations, with the 6-311++G(3df,3pd)

211   basis set, were performed on the studied dispiro-1,2,4-trioxolane (adamantane-2-spiro-3'-8'-

212   oxo-1',2',4'-trioxaspiro[4,5]decane; **1**). Both methods predict the existence of two

213   conformers of the compound with similar energies (see Table 1), which are represented in

214   Figure 1. The two conformers differ in the orientation of the spiro-*p*-cyclohenananonyl moiety,

215   which in the most stable form (A) is turned to the peroxide group and in the less stable one

216   (B) is oriented towards the ring ether fragment. Their population ratio (A:B) in the room

7

217 temperature (298.15 K) gas phase equilibrium is expected to stay between 1.1 and 1.5 (which

218 are the values resulting from the relative energies obtained in the B3LYP and M06-2X

219 calculations, respectively), *i.e.*, both forms are predicted to be significantly populated in these

220 experimental conditions, and can then be expected to be present in the cryogenic matrices

221 investigated in this work (see below). The Cartesian coordinates of the two conformers, as

222 predicted by the two methods used in this study, are provided as Supporting Information

223 (Tables S1 and S2).

1A   **1B**
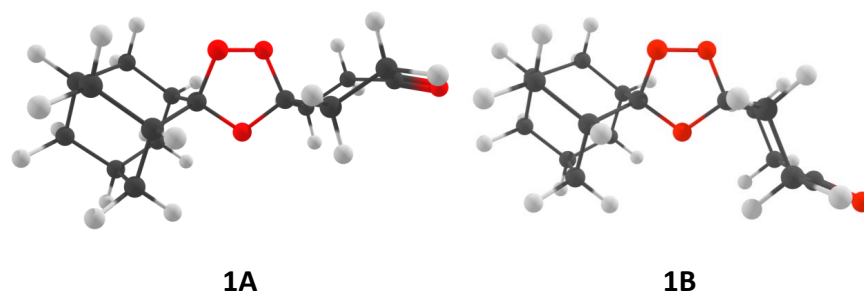
224

225 **Figure 1.** B3LYP/6-311++G(3df,3pd) optimized structures of the two conformers of **1** in the

226 electronic ground state (S_0).

227

228 **Table 1.** B3LYP/6-311++G(3df,3pd) and M06-2X/6-311++G(3df,3pd) calculated energies (kJ mol^{-1}

229) for the conformers of **1** (see Figure 1) zero-point energies (ZPE) and estimated room temperature

230 (298.15 K) percent populations in the gas phase equilibrium.

	B3LYP		**M06-2X**	
	1A	**1B**	**1A**	**1B**
Energy	-2426219.58	-2426218.50	-2425270.01	-2425269.82
ZPE	954.83	954.74	966.62	966.59
Energy (with ZPE)	-2425264.75	-2425263.76	-2424303.39	-2424303.22
ΔEnergy	0.00	0.99	0.00	0.17
Population (298.15 K)	59.8 %	40.2 %	51.7 %	48.3 %

231
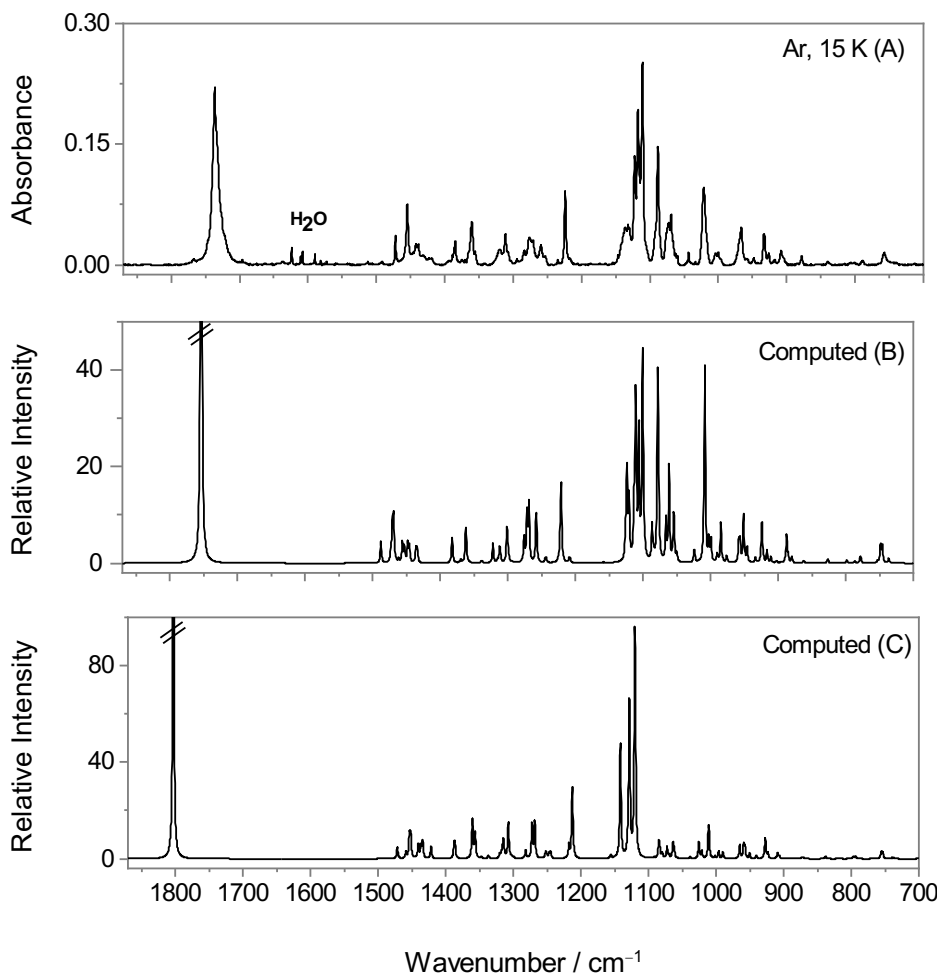
Figure 2. Infrared spectra of **1**: (A) isolated in an Ar matrix (15 K); (B), (C) calculated using the B3LYP and M06-2X functionals (with the 6-311+G(3df,3pd) basis set). The calculated spectra are shown as the 1:1 sum of the spectra of both conformers of the compound, and the frequencies were scaled by 0.983 and 0.971 factors in (B) and (C), respectively. The spectrum observed in the N_2 matrix is very similar to that obtained in argon and is provided in the Supporting Information (Figure S2).

The dispiro-1,2,4-trioxolane **1** was sublimed under high-vacuum at room temperature and co-deposited with large excess of argon or N_2 onto the cold (15 K) CsI substrate of the used cryostat. The infrared spectra of the prepared matrices were subsequently recorded. The spectrum obtained for the compound in the argon matrix is shown in Figure 2, while that obtained in the N_2 matrix is provided in the Supporting Information (Figure S2). The two spectra were found to be very similar, testifying the fact that the molecules of the compound were well-isolated in both matrices and also that the conformational population of **1** existing in the gas phase prior to deposition was efficiently trapped in the matrices. Also, the peroxide

9

247   **1** was found not to undergo thermal decomposition upon sublimation under the used

248   conditions for matrix deposition. The spectroscopic data (both experimental and calculated

249   frequencies and intensities) are summarized in Tables S3-S5 (Supporting Information). It can

250   be seen that, in spite of the similarity of the spectra of the two conformers, several bands

251   observed in the experimental spectra could be assigned to the individual forms, thus

252   confirming the presence of both conformers in the matrices.

253   The comparison of the spectrum obtained in the argon matrix with those theoretically

254   predicted (see Figure 2), shows that the B3LYP functional reproduces better the experimental

255   data throughout the spectrum than the M06-2X functional. Thus, spectra calculated using the

256   B3LYP functional will be used in this study for the analysis of the experimentally obtained

257   spectroscopic data of the remaining compounds under study.

258   The UV-induced reactivity of **1** was investigated in the two types of matrices used (Ar,

259   N_2). Argon matrix was used as standard work medium, while N_2 matrix, known to stabilize

260   high-energy species by establishing specific interactions with the guest species[45,46], was

261   chosen to check the possibility of detection in this medium of any putative reaction

262   intermediate. Both broadband ($\lambda \geq 290$ nm) and narrowband ($\lambda = 290$ nm) excitations were

263   applied. The irradiations were performed at wavelengths within the observed band in the UV-

264   vis spectra of **1** in ethanol solution (Figure S3). The results were found to be qualitatively

265   identical in both matrices and for the two excitation procedures followed. Upon excitation,

266   the bands initially present in the spectra reduced in intensity, while new bands started to

267   emerge, indicating conversion of the trioxolane **1** into other chemical species. Particularly

268   noticeable new spectral features were observed in the ν(C=O), (between 1720-1750

269   cm^{-1}) and ν(C-O), (1080-1120 cm^{-1}) regions. The intensities of the bands of **1** and those of

270   the new bands changed continuously with the irradiation time, until almost complete

271   conversion of the reactant **1** (after ~30 min. of broadband irradiation of the compound in an

272   argon matrix). Detailed analysis of the spectra of the photolysed matrices allowed

273   identification of the observed photolysis products as being 4-oxahomoadamantan-5-one **4**

274   and 1,4-cyclohexanedione **5**, the expected final products for the photolysis of the trioxolane

275   **1**, initiated by homolytic cleavage of the labile peroxide bond. This can be clearly seen in

276   Figure 3, where the experimental difference IR spectrum (spectrum obtained after 30 min. of

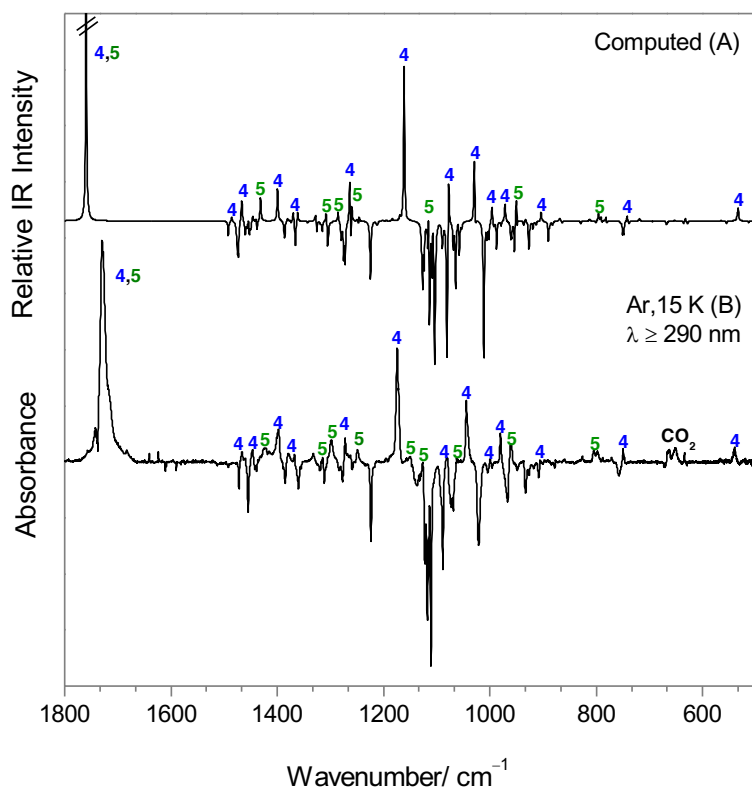277   irradiation at $\lambda \geq 290$ nm *minus* spectrum of the as-deposited argon matrix) is compared with

278   the B3LYP/6-311++G(3df,3pd) calculated difference IR spectrum generated by subtracting

279   the calculated spectrum of **1** from the sum of the spectra of **4** and **5** {in a ratio

280   (0.5[**4**]+0.5[**5**]):1[**1**]}. The identification of the photoproducts was further confirmed by

281   recording the IR spectra of genuine samples of **4** and **5** (see experimental section) deposited

282   in argon matrices and *(i)* comparing these spectra with the spectra of the photoproducts

283   generated upon UV irradiation of matrix isolated **1** (see Figure 4), or *(ii)* comparing the

284   difference experimental IR spectrum shown in Figure 3 (irradiated *minus* as-deposited matrix

285   spectra) with the one obtained by subtracting the experimental spectrum of **1** from the sum

286   of the experimentally obtained IR spectra of the genuine samples of **4** and **5** isolated in argon

287   matrices (see Figure 5).

288   The structural computed data obtained with the B3LYP and M06-2X functionals for **4**

289   and **5** (graphical representation of the optimized minimum energy structures, and summary

290   of calculated energy data), as well as the spectroscopic data obtained both theoretically and

291   experimentally for these compounds (graphical comparison of the calculated and matrix

292   isolation experimental infrared spectra of the compounds, and tables with calculated and

293   experimental frequencies and intensities, those latter including the bands of **4** and **5** both in

294   the photolysed matrices of **1** and as isolated species) are given in the Supporting Information

295   (Tables S6-S14 and Figures S4 and S5). The B3LYP computed vibrational frequencies of **4** and

296   **5** were scaled by 0.983 and 0.982, respectively.

297   According to the obtained results, the diradical rearrangement is regioselective, with no

298   evidence of formation of the alternative products, 2-adamantanone and oxocane-2,7-dione.

299   This can be clearly seen when one compares the infrared spectra of the photoproduced

300   species, generated after UV irradiation of the matrix-isolated **1**, with those of 2-

301   adamantanone and oxocane-2,7-dione (see Figure 3; additional calculated structural and

302   spectroscopic data on these two compounds are presented in the Supporting Information,

303   Figure S6 and Tables S15 and S16). The observed regioselectivity can be explained by the

304   expected greater stability of the (secondary carbon-centered)/oxygen-centered diradical

305   species **3**, in comparison with the putative alternative (primary carbon-centered)/oxygen-

306   centered diradical that would lead to the non-observed final products. In addition, spin

307   density calculations (performed at the B3LYP/6-311++G(3df,3dp) level) on the triplet state

308   dioxygen-centered diradical result in a considerable larger electron spin density in the tertiary

309 β-carbon of the spiroadamantyl substituent as compared to that of the secondary β-carbon of

310 the spiro-*p*-cyclohexanonyl substituent, which can also be considered an indication of a most

311 favorable rearrangement of the initially generated dioxygen-centered diradical into the

312 (secondary carbon-centered)/oxygen-centered diradical species **3**, leading to the observed

313 final products.

314

315

316 **Figure 3**. (A) B3LYP/6-311++G(3df,3pd) calculated difference IR spectrum: spectra of 4-

317 oxahomoadamantan-5-one **4** and 1,4-cyclohexanedione **5** *minus* the spectrum of **1** [in a ratio

318 (0.5+0.5):1]. (B) Experimental difference IR spectrum: spectrum after irradiation at λ ≥ 290 (30 min.;

319 Ar matrix at 15 K) *minus* spectrum of the as-deposited matrix. The negative bands were assigned to

320 **1**; the positive ones were assigned to the new photogenerated species **4** and **5**.

321
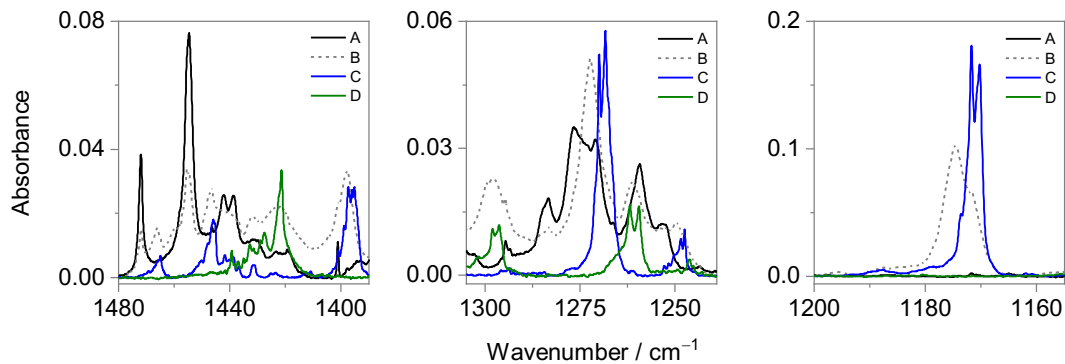
322

323 **Figure 4**. Comparison of selected regions of the experimental IR spectrum obtained before irradiation

324 of the matrix isolated **1** (Ar matrix at 15 K) (solid black line; A) with the spectrum collected after 30

325 min of $\lambda \geq 290$ irradiation (dashed gray line; B) and with the spectra of authentic samples of 4-

326 oxahomoadamantan-5-one **4** (solid blue line; C) and 1,4-cyclohexanedione **5** (solid green line; D)

327 isolated in argon at 15 K.

328
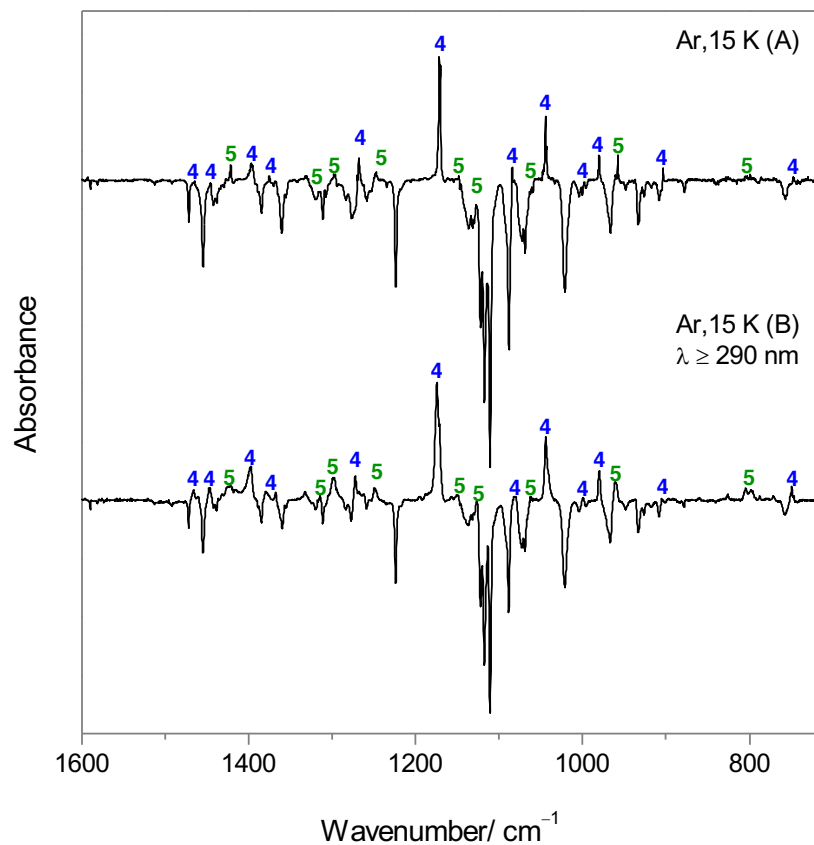
329

330 **Figure 5**. (A) Experimental difference IR spectrum: spectra of authentic samples of matrix isolated

331 4-oxohomoadamantan-5-one **4** and authentic 1,4-cyclohexanedione **5** *minus* spectrum of **1**   Ar

13

332   matrix at 15 K). (B) Experimental difference IR spectrum: spectrum after irradiation of matrix

333   isolated **1** (λ ≥ 290; 30 min) *minus* spectrum of the as-deposited matrix (Ar matrix at 15 K).

334

335   ***EPR detection of the dioxygen-centered 2 and carbon-centered/oxygen-centered 3***

336   ***diradicals***

337   The *in situ* EPR measurements in the photolysis of **1** in MeTHF matrix were conducted

338   using 266 nm laser light (5 mJ) at 10-50 K. The X-band EPR signals were measured at a

339   resonance frequency of 9.40 GHz (Figure 6). During the photolysis at 10 K (Figure 6 Ib), a

340   half-field signal at ~1550 G (triplet species A) was observed after 120 seconds, which is a

341   typical triplet species of diradicals, and another half-field signal at 1670 G (triplet species B)

342   was detected after 420 seconds, together with the 1550 G signal (Figure 6 Ic). Both resonance

343   frequencies (1550 and 1670 GHz) are typical for triplet diradicals. Under dark conditions,

344   only the half-field signal at 1670 G was detected (Figure 6 Id), indicating that the disappeared

345   triplet species A is short-lived, while the triplet species B is persistent, under the MeTHF
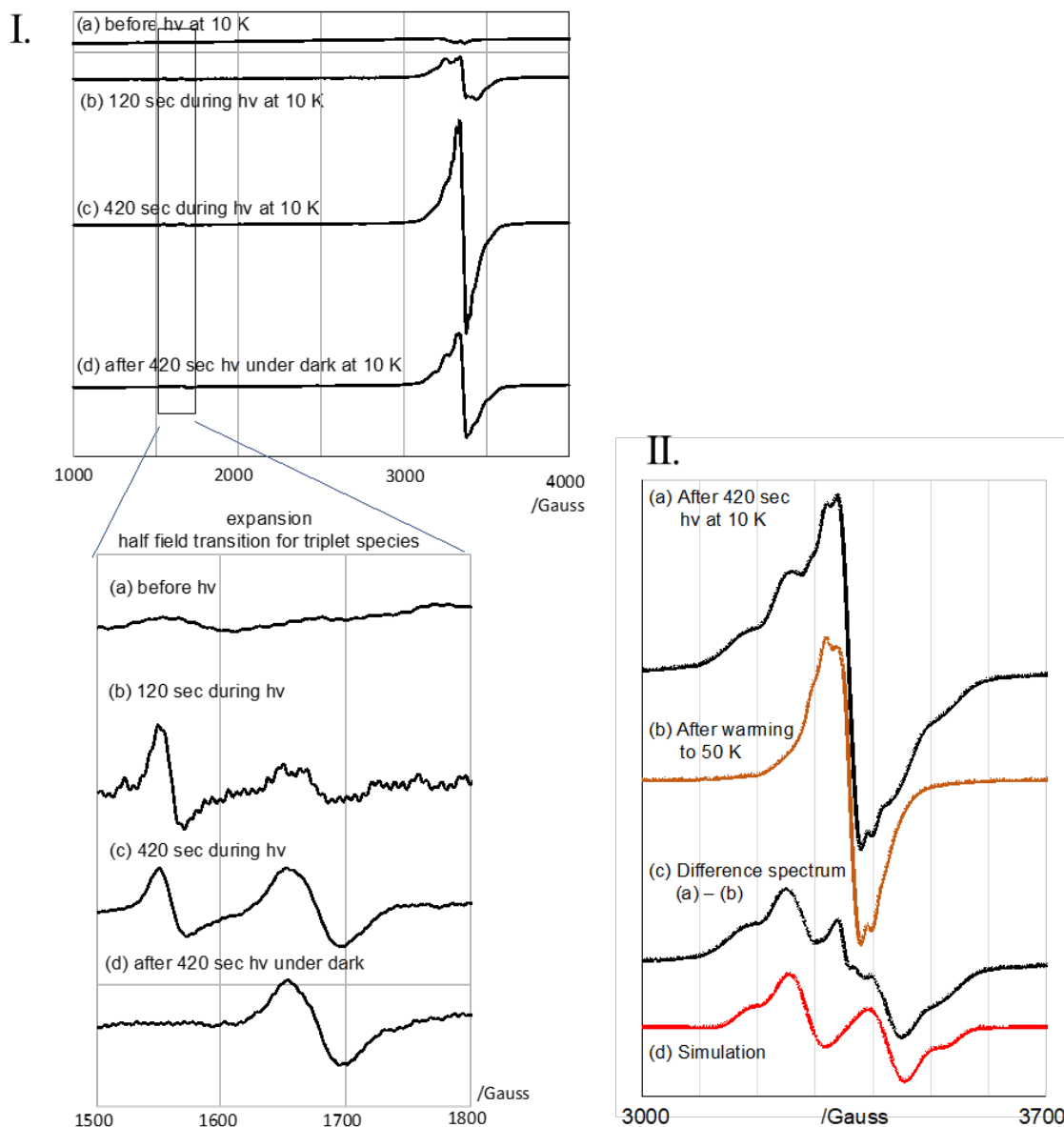
346   matrix conditions, at 10 K.

Figure 6. **I**: X-band EPR spectra (9.40 GHz, 1000-4000 G) obtained from photolysis studies of compound 1 (100 mM) in MeTHF-matrix, at 266 nm; (a) before irradiation at 10 K; (b) after irradiation for 120 seconds at 10 K; (c) after irradiation for 420 seconds, at 10 K; (d) after irradiation for 420 seconds, under dark, at 10 K; **II**: X-band EPR signals (9.40 GHz, 3000-4000 G) from photolysis of compound **1** (100 mM) in MeTHF-matrix at 266 nm; (a) after 420 seconds photolysis, under dark, at 10 K; (b) after warming the sample to 50 K, and subsequent re-cooling to 10K; (c) difference spectrum between (a)–(b); (d) simulated spectrum with $D/hc = 0.160$ cm^{-1} and $E/hc = 0.001$ cm^{-1} at g value of 2.003.

357   To gather further insight regarding the reactivity of the triplet species B, the photolysate

358   at 10 K was warmed to 50 K under dark conditions (Figure 6 IIb). The typical triplet signal

359   disappeared and did not recover to the original one in Figure 6 Ic after re-cooling the sample

360   to 10 K, indicating that the triplet species B was also thermally labile at ~50 K. The triplet

361   signal of B was obtained by the difference spectrum of Figure 6 IIa–b (Figure 6 IIc). The

362   zero-field splitting parameters D/hc and E/hc of the triplet species B were determined to be

363   0.160 cm^{-1} and 0.001 cm^{-1} after the simulation (Figure 6 IId). From the D/hc value, the

364   distance between two spins was estimated to be ~ 5 Å.

365   The EPR results demonstrate that two triplet species (A and B) are formed during the

366   photolysis of the studied trioxolane **1**, in agreement with the expectations. One of the triplet

367   species (A) is thermally quite labile, while the other (B) is persistent at 10 K. Considering

368   the results obtained in the photolysis of **1** in argon matrix, in particular the obtained final

369   products, the theoretical data described in the previous sections, and the accumulated

370   literature evidence, diradicals **2** and **3** shall be assigned to the intermediates A and B,

371   respectively, detected by EPR. This is the first experimental detection of these diradical

372   intermediates.

373

374   **CONCLUSIONS**

375   Adamantane-2-spiro-3'-8'-oxo-1',2',4'-trioxaspiro[4,5]decane **1**, a reported potent

376   antiparasitic dispiro-1,2,4-trioxolane, has been synthesized and studied from the view point

377   of its molecular structure and monomeric photochemistry, using matrix isolation techniques

378   coupled to FTIR and EPR spectroscopy. It is noteworthy that the ozonide **1** remained

379   thermally stable upon sublimation required for matrix deposition. All experimental results

380   have been supported by quantum chemical calculations using two levels of theory [B3LYP/6-

381   311++G(3df,3dp) and M06-2X/6-311++G(3df,3dp)], the comparison of the spectrum

382   obtained in the argon matrix with those theoretically predicted showing that the B3LYP

383   functional reproduces better the experimental data throughout the spectrum than the M06-

384   2X functional. Both methods predict two conformers for the dispiro-1,2,4-trioxolane **1** with

385   very close energies, differing in the orientation of the spiro-p-cyclohenanonyl moiety, which

386   in the most stable form is directed to the peroxide group, while in the less stable one is

387   oriented towards the ring ether fragment. In the experimental spectra, several bands were

388   observed which permitted the assignment of the individual forms, thus confirming the

389   presence of both conformers in the matrices.

390   The UV-induced reactivity of **1** was investigated in the two types of matrices (Ar, N_2),

391   using broadband ($\lambda \geq 290$ nm) and narrowband ($\lambda = 290$ nm) irradiation, the results proving

392   qualitatively identical in both matrices and for the two followed excitation procedures.

393   Irradiation of matrix-isolated **1** at $\lambda \geq 290$ nm resulted in photocleavage of the trioxolane

394   pharmacophore with formation of other chemical species, as evidenced by the observation of

395   new spectral features in the ν(C=O), (between 1720-1750 cm^{-1}) and ν(C-O), (1080-1120 cm^{-1})

396   ^{1}) regions. Detailed analysis of the spectra of the photolyzed matrices allowed identification

397   of 4-oxahomoadamantan-5-one **4** and **1**,4-cyclohexanedione **5** as the sole final products from

398   photolysis of the trioxolane **1**. This identification was further confirmed through comparison

399   with the matrix spectra of the pure compounds. Such observation indicates that the dioxygen-

400   centered diradical **2**, formed upon homolytic cleavage of the labile peroxide bond, undergoes

401   a regioselective radical isomerization to form the more stable (secondary carbon-

402   centered)/oxygen-centered diradical **3**. In fact, no evidence was observed for the formation

403   of 2-adamantanone and oxocane-2,7-dione, the products that would arise from the putative

404   alternative (primary carbon-centered)/oxygen-centered diradical. The observed

405   regioselectivity can be explained by the expected greater stability of the (secondary carbon-

406   centered)/oxygen-centered diradical species **3** in comparison to its primary counterpart. Spin

407   density calculations (performed at the B3LYP/6-311++G(3df,3dp) level) on the triplet state

408   dioxygen-centered diradical result in a considerably larger electron spin density in the tertiary

409   β-carbon of the spiroadamantyl substituent as compared to that of the secondary β-carbon of

410   the spiro-*p*-cyclohexanonyl substituent, which can also be taken as an indication of a most

411   favorable rearrangement of the initially generated dioxygen-centered diradical into the

412   (secondary carbon-centered)/oxygen-centered diradical species **3**, leading to the final

413   products identified. These results are in keeping with information gathered from studies on

414   the mechanisms of bioactivation and action of trioxolane based antiparasitic candidates,

415   where heme-adducts of the secondary carbon-centered)/oxygen-centered diradical species

416   analogues of **3** were detected[47].

417   *In situ* EPR measurements during photolysis of compound **1** deposited in a MeTHF-

418   matrix led to the detection of signals at1550 and 1670 GHz, corresponding to resonances of

419 two triplet diradicals, the one at 1550 GHz appearing thermally labile while the other (1670

420 GHz) proved persistent at 10 K. The observation of signals with resonance frequencies that

421 are typical for triplet diradicals, combined with the product characterizations achieved

422 through the matrix isolation FTIR studies, indicate that the postulated diradicals **2** and **3** shall

423 correspond to the intermediates detected by the experiment.

424   In conclusion, our results support the proposal of a regioselective radical isomerization

425 of dioxygen-centered diradical **2** to afford the (secondary carbon-centered)/oxygen-centered

426 diradical **3**, also providing evidence for the presence of both intermediate diradicals on a

427 photolyzed MeTHF-matrix containing compound **1**. This work deepens the knowledge

428 concerning the photoreactivity/photostability of antiparasitic endoperoxides based on the

429 trioxolane pharmacophore.

430

431 **ASSOCIATED CONTENT**

432 Supporting Information. Supplemental figures and calculated data for adamantane-2-spiro-

433 3'-8'-oxo-1',2',4'-trioxaspiro[4,5]decane. This material is available free of charge via the

434 Internet at http://pubs.acs.org

435

436 **AUTHOR INFORMATION**

437 **Corresponding Author**

438 * E-mail: rfausto@ci.uc.pt

439 * E-mail: mcristi@ualg.pt

440 Notes

441 The authors declare no competing financial interest.

442 **Author Contributions**

443 The authors contributed equally.

444

445

446

455

REFERENCES

457 1. Tu, Y. Y. The discovery of artemisinin (qinghaosu) and gifts from Chinese medicine,

458   *Nature Med.*, **2011**, *17*, 1217–1220.

459 2. Tu, Y. Y. Artemisinin - A Gift from Traditional Chinese Medicine to the World

460   (Nobel Lecture). *Angew. Chem. Int. Ed.*, **2016**, *55*, 10210–10226.

461 3. Liu, C. X. Discovery and Development of Artemisinin and Related Compounds.

462   *Chin. Herb. Med.*, **2017**, *9*, 101–114.

463 4. Jefford C. W. Why Artemisinin and Certain Synthetic Peroxides are Potent

464   Antimalarials. Implications for the Mode of Action. *Curr. Med. Chem.*, **2011**, *8*,

465   1803–1826.

466 5. Cumming, J. N.; Polypradith, P.; Posner, G. H. Antimalarial Activity of Artemisinin

467   (Qinghaosu) and Related Trioxanes: Mechanism(s) of Action. *Adv. Pharmacol.*,

468   **1996**, *37*, 253–297.

469 6. Wu, Y. How Might Qinghaosu (Artemisinin) and Related Compounds Kill the

470   Intraerythrocytic Malaria Parasite? A Chemist's View. *Acc. Chem. Res.*, **2002**, *35*,

471   255–259.

472 7. Robert, A.; Coppel, Y.; Meunier, B. Alkylation of heme by the antimalarial drug

473   artemisinin. *Chem. Commun.*, **2002**, 414–415.

474 8. Meshnick, S. R.; Artemisinin: mechanisms of action, resistance and toxicity. *Int. J.

475   Parasitol.*, **2002**, *32*, 1655–1660.

476 9. Eckstein-Ludwig, U.; Krieger, J.; Smeilus, T.; Kaiser, M.; Seo, E. J.; Efferth, T.;

477   Ginannis, A. Total Synthesis and Biological Investigation of (-)-Artemisinin: The

478   Antimalarial Activity of Artemisinin Is not Stereospecific. *Angew. Chem. Int. Ed.*,

479   **2018**, *57*, 8293–8296.

19

480   10. Tilley, L.; Straimer, J.; Gnädig, N. F.; Ralph, S. A.; Fidock, D. A. Artemisinin Action

481   and Resistance in *Plasmodium falciparum*. *Trends Parasit.*, **2016**, *32*, 682–696.

482   11. Winzeler, E. A.; Manary, M. J. Drug resistance genomics of the antimalarial drug

483   artemisinin. *Gen. Biol.*, **2014**, *15*, 544.

484   12. Cravo, P.; Napolitano, H.; Culleton, R. How genomics is contributing to the fight

485   against artemisinin-resistant malaria parasites. *Acta Tropica*, **2015**, *148*, 1–7.

486   13. Wang, J.; Zhang, C.; Chia, W.; Loh, C.; Li, Z.; Lee, Y.; He, Y.; Yuan, L.; Lim, T.;

487   Liu, M. et al. Haem-activated promiscuous targeting of artemisinin in *Plasmodium*

488   *falciparum*. *Nature Comm.*, **2015**, *6*, Art. Nº 10111 (1–11).

489   14. Aweeka, F. T.; German, P. I. Clinical Pharmacology of Artemisinin-Based

490   Combination Therapies. *Clin. Pharmacokin.*, **2008**, *47*, 91–102.

491   15. Sugimone, H. H. In *Handbook of Organic Photochemistry and Photobiology*.

492   Horspool, W. M.; Song, P. S. Eds.; CRC Press, London, **1994**, pp 1229–1253

493   references therein.

494   16. Jefford, C. W.; Rossier, J. C.; Boukouvalas, J. Eliminative ring fission of 1,2,4-

495   trioxan-5-ones. A new approach to α-keto acids. *J. Chem. Soc. Chem. Commun.*,

496   **1986**, 1701–1702.

497   17. Jefford, C. W.; Rossier, J. C.; Boukouvalas, J. A Mild and Efficient Preparation of

498   cis-1,2-Diols from 1,2,4-Trioxanes. *J. Chem. Soc. Chem. Commun.*, **1987**, 1593–

499   1594.

500   18. Jefford, C. W.; Kohmoto, S.; Rossier, J. C.; Boukouvalas, J. Chemistry of 1,2,4-

501   Trioxanes. Formation of 1,2-Diol Monoesters. *J. Chem. Soc. Chem. Commun.*, **1985**,

502   1783–1784.

503   19. Jefford, C. W.; Rossier, J. C.; Boukouvalas, J. 1,2,4-Trioxanes as masked, dual

504   purpose, functional groups. *Heterocycles*, **1989**, *28*, 673–676.

505   20. Jefford, C. W.; Rossier, J. C.; Boukouvalas, J. Electrophile-induced rearrangement of

506   1,2,4-trioxanes. Formation of 1-benzofuran and 2H-1-benzopyrans. *J. Chem. Soc.*

507   *Chem. Commun.*, **1987**, 713–714.

508   21. Erhardt, S.; Macgregor, S. A.; McCullough, K. J.; Savill, K.; Taylor, B. J. Model

509   Studies of β-Scission Ring-Opening Reactions of Cyclohexyloxy Radicals:

510   Application to Thermal Rearrangements of Dispiro-1,2,4-trioxanes. *Org. Lett.*, **2007**,

511   *9*, 5569–5572.

22. Tang, Y.; Dong, Y.; Wang, X.; Sriraghavan, K.; Wood, J. K.; Vennerstrom J. L.

513   Dispiro-1,2,4-trioxane   Analogues   of   a   Prototype   Dispiro-1,2,4-trioxolane:

514   Mechanistic Comparators for Artemisinin in the Context of Reaction Pathways with

515   Iron(II). *J. Org. Chem.*, **2005**, *70*, 5103–5110.

23. Haq, A.; Kerr, B.; McCullough K. J. A Rapid Route to Medium to Large Ring

517   Lactones via the Thermolysis of Dispiro-1,2,4-trioxane Derivatives. *J. Chem. Soc.*

518   *Chem. Commun.*, **1993**, 1076–1078.

24. Abe, M.; Adam, W.; Heidenfelder, T.; Nau, W. M.; Zhang, X.; Intramolecular and

520   Intermolecular Reactivity of Localized Singlet Diradicals: The Exceedingly Long-

521   Lived 2,2-Diethoxy-1,3-diphenylcyclopentane-1,3-diyl. *J. Am. Chem. Soc.*, **2000**,

522   *122*, 2019–2026.

25. Abe, M.; Inakazu, T.; Munakata, J.; Nojima, M. ^{18}O-Tracer Studies of Fe(II)-Induced

524   Decomposition of 1,2,4-Trioxolanes (Ozonides) Derived from Cyclopentenes and

525   Indenes. Inner-Sphere Electron Transfer Reduction of the Peroxide Linkage. *J. Am.*

526   *Chem. Soc.*, **1999**, *121*, 6556–6562.

26. Meyer, B. *Low Temperature Spectroscopy*, American Elsevier Publishers Company;

528   New York (USA), **1971**.

27. Andrews L.; Moskovits, M. *Chemistry and Physics of Matrix Isolated Species*. Eds.,

530   Elsevier, Amsterdam (Holland), **1989**.

28. Barnes, A.; Orville-Thomas, W. J.; Gaufrhs, R.; Muller, A. *Matrix Isolation*

532   *Spectroscopy*. Eds.; Springer; Dordrecht (Holland), **1981**.

29. Dunkin, I. R. *Matrix Isolation Techniques: A Practical Approach*. Oxford University

534   Press; Oxford (UK), **1998**.

30. Fausto, R. *Low Temperature Molecular Spectroscopy*. Ed., NATO-ASI Series C483;

536   Kluwer, Amsterdam (Holland), **1996**.

31. Vennerstrom, J. L.; Dong, Y.; Chollet, J.; Matile, H. Spiro and dispiro 1,2,4-

538   trioxolane antimalarials. U.S. patent. 6,486,199B1, **2002**.

32. Lobo, L.; Cabral, L. I. L.; Sena, M. I.; Guerreiro, B. Rodrigues, A. S.; Andrade-Neto,

540   V. F.; Cristiano, M. L. S.; Nogueira, F. New endoperoxides highly active *in vivo* and

541   *in vitro* against artemisinin-resistant *Plasmodium falciparum*. *Malar. J.*, **2018**, *17*, 1–

542   11.

543   33. Cortes, S.; Albuquerque, A.; Cabral, L. I. L.; Lopes, L.; Campino, L.; Cristiano, M.

544   L. S. *In vitro* susceptibility of *Leishmania infantum* to Artemisinin derivatives and

545   selected trioxolanes. *Antimicrob. Agents Chemother*. **2015**, *59*, 5032–5035.

546   34. Araujo, N.C.P.; Afonso, R.; Beringela, A.; Cancela, M.L.; Cristiano, M.L.S.; Leite,

547   R.B. Peroxides with antiplasmodial activity inhibit proliferation of *Perkinsus olseni*,

548   the causative agent of Perkinsosis in bivalves. *Parasitol. Int*., **2013**, *62*, 575–582.

549   35. Renoud-Grappin, M.; Vanucci, C.; Lhommet, G. Diastereoselective synthesis of a

550   limonoid model related to the insect antifeedant genudin. *J. Org. Chem*., **1994**, *59*,

551   3902–3905.

552   36. Raghavachari, K.; Binkley, J. S.; Seeger, R.; Pople, J. A. Selfconsistent molecular

553   orbital methods. XX. A basis set for correlated wave functions. *J. Chem. Phys*., **1980**,

554   *72*, 650–654.

555   37. Frisch, M. J.; Pople, J. A.; Binkley, J. S. Selfconsistent molecular orbital methods 25.

556   Supplementary functions for Gaussian basis sets, *J. Chem. Phys*., **1984**, *80*, 3265–69.

557   38. Becke, A. D. Density-functional thermochemistry. III. The role of exact exchange. *J.*

558   *Chem. Phys*., **1993**, *98*, 5648–5652.

559   39. Lee, C.; Yang, W.; Parr, R. G. Development of the Colic-Salvetti correlation-energy

560   formula into a functional of the electron density. *Phys. Rev. B*, **1988**, *37*, 785–789.

561   40. Vosko, S. H.; Wilk, L.; Nusair, M. Accurate spin-dependent electron liquid

562   correlation energies for local spin density calculations: a critical analysis. *Can. J.*

563   *Phys*., **1980**, *58*, 1200–1211.

564   41. Stephens, P. J.; Devlin, F. J.; Chabalowski, C. F.; Frisch, M. J. F. *Ab Initio*

565   Calculation of Vibrational Absorption and Circular Dichroism Spectra Using Density

566   Functional Force Fields. *J. Phys. Chem*., **1994**, *98*, 11623–11627.

567   42. Zhao, Y.; Truhlar, D. G. The M06 suite of density functionals for main group

568   thermochemistry, thermochemical kinetics, noncovalent interactions, excited states,

569   and transition elements: two new functionals and systematic testing of four M06-class

570   functionals and 12 other functionals. *Theor. Chem. Acc*., **2008**, *120*, 215–241.

571 43. Zhao, Y.; Truhlar, D. G. Density Functionals with Broad Applicability in Chemistry.

572 *Acc. Chem. Res.*, **2008**, *41*, 157–167.

573 44. Frisch, M. J.; Trucks, G. W.; Schlegel, H. B.; Scuseria, G. E.; Robb, M. A.;

574 Cheeseman, J. R.; Scalmani, G.; Barone, V.; Mennucci, B.; Petersson, G. A. et al.

575 Gaussian 09, Revision D.01; Gaussian, Inc.; Wallingford, CT, **2004**.

576 45. Lopes, S.; Domanskaya, A. V.; Fausto, R.; Räsänen, M.; Khriachtchev, L. Formic

577 and acetic acids in a nitrogen matrix: Enhanced stability of the higher-energy

578 conformer. *J. Chem. Phys.*, **2010**, *133*, 144507.

579 46. Kus, N.; Fausto R. Effects of the matrix and intramolecular interactions on the

580 stability of the higherenergy conformers of 2-fluorobenzoic acid. *J. Chem. Phys.*,

581 **2017**, *146*, 124305.

582 47. Gibbons, P.; Verissimo, E.; Araujo, N. C.; Barton, V.; Nixon, G. L.; Amewu, R. K.;

583 Chadwick, J.; Stocks, P. A.; Biagini, G. A. B.; Srivastava, A. et al. Endoperoxide

584 Carbonyl Falcipain 2/3 Inhibitor Hybrids: Toward Combination Chemotherapy of

585 Malaria through a Single Chemical Entity. *J. Med. Chem.*, **2010**, *53*, 8202-8206.

586
587